

# Extensible Structure-Informed Prediction of Formation Energy with Improved Accuracy and Usability employing Neural Networks

Adam M. Krajewski<sup>a</sup>, Jonathan W. Siegel<sup>b</sup>  
Jinchao Xu<sup>b</sup>, Zi-Kui Liu<sup>a</sup>

a. Department of Materials Science and Engineering, The Pennsylvania State University, USA

b. Department of Mathematics, The Pennsylvania State University, USA

Corresponding author: A. M. Krajewski, 216-456-1534, ak@psu.edu

November 2, 2022

## Abstract

In recent years, numerous studies have employed machine learning (ML) techniques to enable orders of magnitude faster high-throughput materials discovery by augmentation of existing methods or as standalone tools. In this paper, we introduce a new neural network-based tool for the prediction of formation energies based on elemental and structural features of Voronoi-tessellated materials. We provide a self-contained overview of the ML techniques used. Of particular importance is the connection between the ML and the true material-property relationship, how to improve the generalization accuracy by reducing overfitting, and how new data can be incorporated into the model to tune it to a specific material system.

In the course of this work, over 30 novel neural network architectures were designed and tested. This led to three final models optimized for (1) highest test accuracy on the Open Quantum Materials Database (OQMD), (2) performance in the discovery of new materials, and (3) performance at a low computational cost. On a test set of 21,800 compounds randomly selected from OQMD, they achieve mean average error (MAE) of 28, 40, and 42 meV/atom respectively. The second model provides better predictions on materials far from ones reported in OQMD, while the third reduces the computational cost by a factor of 8.

We collect our results in a new open-source tool called SIPFENN (Structure-Informed Prediction of Formation Energy using Neural Networks). SIPFENN not only improves the accuracy beyond existing models but also ships in a ready-to-use form with pre-trained neural networks and a user interface.

# Contents

<b>1</b>	<b>Introduction</b>	<b>3</b>
1.1	Motivation . . . . .	3
1.2	Approach . . . . .	4
<b>2</b>	<b>Methodology</b>	<b>6</b>
2.1	Descriptor Used . . . . .	6
2.2	Machine Learning Techniques Overview . . . . .	8
2.2.1	Regression Problem Formulation . . . . .	9
2.2.2	Artificial Neural Networks . . . . .	10
2.2.3	Overfitting . . . . .	11
2.2.4	Overfitting Mitigation . . . . .	13
2.2.5	Transfer Learning . . . . .	15
2.3	Software Used . . . . .	15
2.4	Data Acquisition and Curation . . . . .	16
2.5	Neural Network Design Process and Intermediate Results . . . . .	16
<b>3</b>	<b>Results</b>	<b>20</b>
3.1	Final Predictive Models . . . . .	20
3.2	OQMD Data Performance . . . . .	22
3.3	Non-OQMD Data Performance . . . . .	22
3.4	Transfer Learning Capability . . . . .	24
3.5	End-User Implementation - SIPFENN . . . . .	26
<b>4</b>	<b>Conclusions</b>	<b>28</b>
4.1	Summary of Results and Significance . . . . .	28
4.2	Software Access . . . . .	29
4.3	Acknowledgements . . . . .	29
<b>5</b>	<b>References</b>	<b>30</b>

# 1 Introduction

## 1.1 Motivation

In recent years the field of material data informatics has been growing in importance thanks to the growing number of open-access databases [1–7] and new methods being implemented to predict a wide variety of material properties [?, 8–16]. Within these methods, machine learning (ML) and, more broadly artificial intelligence (AI) is becoming dominant, as noted in two excellent reviews conducted in 2019 [17, 18], which listed a total of around 100 recent studies that attempted to solve tens of different material science problems using ML and AI techniques. These studies report benefits such as a 30-fold increase in material discovery rate when guided by an ML-model [14], or the ability to create new state-of-the-art materials in highly complex design spaces like 6-component alloys [15]. These studies also dive into new paradigms of materials science by handling previously unthinkable amounts of data, allowing the creation and analysis of an energy convex-hull calculated for all elements [19, 20], or a concurrent analysis of all available literature texts to find paths for material synthesis [21]. In addition, some studies promise to solve significant industrial challenges such as detection of additive manufacturing flaws with relatively simple and accessible data, but above-human pattern recognition quality and speed [16].

Within these studies, the majority focus on the discovery of candidate materials promising a new state-of-the-art performance. It is essential, however, to recognize that many of these studies propose hypothetical materials by defining an allowed design search space and then looking for local or global maxima in a utility function, which describes arbitrarily defined desirability. This can simply be the target property or a more robust representation accounting for factors such as model confidence or approximated manufacturing cost. Once prediction results are obtained, they are later passed to experimental groups that attempt to confirm or refute them. This overall process is, however, prone to finding that predictions did not meet expectations due to two main issues. The first stems from the fact that the newly designed materials are usually an extrapolation from already known materials. If the design space is large relative to available data or high dimensional, it is very likely that the model will sharply diverge from the truth in some regions or dimensions. This, combined with preferential treatment of regions with extraordinary predictions, often leads researchers to select such high-divergence regions that produce excellent results in the model. This problem is due to overfitting, and we explicitly address methods for mitigating it in our work.

However, even if the model could always predict true properties, there would be a second, more fundamental issue, namely that the predicted materials often cannot be physically made and experimentally tested. An increasing number of studies attempt to solve this challenge by focusing not only on predicting how the material will perform, but also whether it can be manufactured and then maintain performance [22]. Generally, such studies include predicting materials’ stability [20, 23, 24] and synthesizability [19, 21, 25]. Out of these two, the stability is the more constraining one, as it determines whether the material could be stable or metastable in the use-conditions, and therefore whether it can be synthesizable. Furthermore,

unlike synthesizability, which is a function of approach (i.e. some pathways allow synthesis and some don't), stability is based on fundamental thermodynamic properties. One of these properties is the formation energy, which relates the energy of the studied phase (arrangement of atoms) to the energy of the most stable phases of elements within the structure at zero temperature.

In this paper, a new ML tool is developed to improve the quality of formation energy predictions and streamline their incorporation into future materials discovery frameworks that aim to screen billions rather than hundreds of candidates available with cost-intensive calculations like first-principles calculations based on the density functional theory (DFT).

## 1.2 Approach

In simple terms, every ML model predicts some property and is composed of three essential elements: a database, a descriptor, and an ML technique (also known as ML algorithm). The first element, databases, contain prior knowledge and are becoming increasingly shared between many studies, thanks to being open-access and often containing orders of magnitude more experimental or computational data than could be feasibly collected for a single study [1–7]. Databases used within this paper are detailed in Section 2.4.

The second element of an ML model is the descriptor (i.e. vector describing the material) which determines a representation of knowledge (from the database) in a way relevant to the problem. It is typically built from many features, also known as attributes or vector components (in more mathematical terms), which usually are determined through domain-knowledge to be relevant. All combined, these features are a representation of some state, whose meaning will be problem-specific. For a material, this state will be the material itself, which can be defined as a point in a multidimensional property space that contains all possible properties. In abstract terms, the material descriptor is a projection of a point in this space onto a subspace of selected properties, which is a subset of known properties, itself is a subset of defined properties, as depicted in Figure 1.1.

When treating materials on the atomic level, descriptors can be generally divided into composition-based (also known as stoichiometric, structure-invariant, or elemental) [9,26–28] and structure-informed [29–31]. The first type usually provides a more compact representation at a much lower computational cost, as calculating a composition-based descriptor is often limited to a simple matrix multiplication (linear map), which weights known elemental properties by the materials stoichiometry. However, such a representation is inherently unusable for prediction of most material properties that depend on the atomic structure. This characteristic makes them, however, notably useful in the case of amorphous materials and other cases where structure is not known. In contrast, the structure-informed descriptors tend to be more robust and more physics-relevant, as they can include much more information related to interatomic interactions. They also, implicitly or explicitly, include symmetries present in the material, which can be used to predict certain properties, such as zero piezoelectric response, with high confidence. Furthermore, such descriptors often include extensive composition-based arguments within them, making it possible to both recognize patterns in the property coming from different chemical species occupying the same



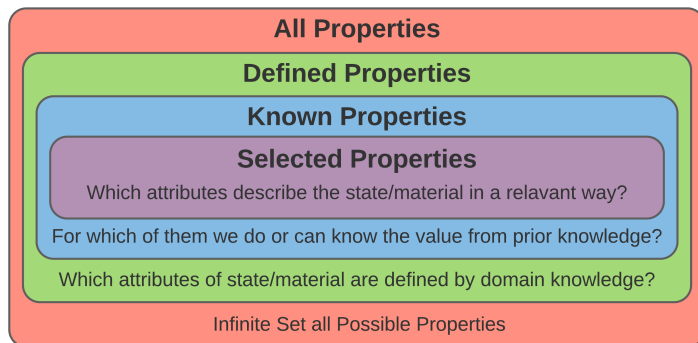


Figure 1.1: Conceptual depiction of how descriptor of a state (e.g. material) is created on a fundamental level. Property is defined when there is a name strictly associated with it (e.g. Young’s Modulus or coordination number). Property is known when its value is known (e.g. 200MPa or 12) or can be derived from known values of other properties. Final selection typically limits such derivations to simple conceptual or computational operations.

structure and structural effects in case of a single composition. This advantage comes at the expense of increased computational cost, however it usually has little impact on the net speed of the model, as the computation time increases from the nanosecond- to millisecond-scale, which is still below execution time of many ML algorithms. This is representative of a the general trade-off between the effectiveness of a descriptor and the computational cost required to compute it.

The current state-of-the-art structure-informed models have been developed by Ward et al. based on information from the Voronoi tessellation of a crystal structure [29]. Ward’s descriptor contains 271 features that combine information from elemental properties of atoms, such as shell occurrences, with information about the their local environments, such as coordination number or bond lengths to neighbours. This approach was demonstrated to work excellently when comprehensively compared to two previous approaches based on the Coulomb matrix (CM) [31] and on the partial radial distribution function (PRDF) [30], when trained on the same (OQMD) data with the same machine learning algorithm. A more detailed overview is given in 2.1, with all features listed in Table 1.

Ward et al. have achieved an excellent prediction quality thanks to good data and an excellent descriptor. However, their approach used a poor ML algorithm, which is one of the essential parts of an ML model. [29] In that work, a random forest algorithm, where output is a superposition of classifying decision trees, is set to an automatic parameter selection. While such an approach is very common in the recent literature, a careful examination of configuration files within the provided supplemental materials reveals that the model is automatically set to unlimited depth (number of decisions in series) and unlimited node count (total number of decisions). These settings, combined with single-datapoint leaves (end values for decision trees), leads to a model composed of 100 trees with approximately 700,000 nodes each (approx.  $N + \frac{1}{2}N + \frac{1}{4}N + \frac{1}{8}N + \dots$ , i.e. twice the size  $N$  of training set). This model requires over 27 GB of RAM memory to run, making it unusable on a typical personal or lab

computer. Such size also results in a relatively large computational cost to make predictions, requiring over 100 ms to run on a high-performance lab computer. [29] Furthermore, since the model can fit data exactly in every tree, this approach is prone to resulting in 100 nearly identical decision trees.

In the present work, all of the aforementioned issues are addressed with a careful manual design of the ML algorithm, which unleashes the full potential knowledge in the data and its representation. This is done by first considering implications of the problem formulation (see 2.2.1) and proposed solution using a deep neural network technique (see 2.2.2). Once the problem is well stated, the solution is found in iterative fashion described in 2.5, by designing and benchmarking the performance of over 50 neural networks belonging to around 30 architectures designed within this study. This approach yields superior results shown in 3.2.

In addition to better performance in relation to the same metrics, there are two other major improvements, obtained by redesigning the ML algorithm as conducted in the present work. The first one is the much improved transfer learning ability, described in 2.2.5. This will allow other researchers, at a relatively small cost, to substantially improve the quality of the model predictions in the design of novel materials that are not similar to what was studied in the past. In a general model this task would lead to significant extrapolations, that in turn tend to reduce both performance and confidence. In the implementation presented here, this is mitigated by the procedure of re-training the model on a small batch of new data with manually modified training behaviour so that the model becomes fine-tuned to the specific material system. At the same time, it retains general knowledge learnt from the large data set, which allows, for example, calculations in which a new element is introduced to the material system. An example of transfer learning and its results, where as little as a few new DFT-calculation datapoints can provide a significant performance increase, is presented in 3.4.

The second major improvement is the end-user usability. While most of the materials-related studies using ML techniques provide excellent descriptions of the designed model and evaluations of its performance, only a small fraction put in an effort beyond making the results reproducible. In contrast, this work has been focused on creating an accessible tool from the beginning, which is described in more detail in 2.3. The result of this is an open-source end-user tool, described in 3.5, that is ready to use without any costly computation and can be run on any modern computer or even a smartphone.

## 2 Methodology

### 2.1 Descriptor Used

As explained in 1.2, a descriptor of a material is a point in a well-defined multidimensional property space that can be used to represent knowledge associated with entries in a database. Within the present work, the property space has 271 dimensions (corresponding to 271 features) related to elemental properties and atomic structure of an arbitrary crystalline

material, which were designed by Ward et al. [27, 29].

The key step in the calculation of a material descriptor, allowing high performance predictions of formation energy, is the inclusion of substantial structural information. This is done through the generation of the Voronoi tessellation of the crystal lattice, which was first used in this context by Ward et al. Their approach utilizes the voro++ code [32] that partitions the space based upon the closest site in the crystal basis and then analyzes attributes of that space region such as volume, numbers and size of faces, and distance from the origin (atom position) to each face. The features used in this work can be divided into the following general categories.

- **Elemental Attributes** (145 total): Attributes which only depend upon the elements present and their stoichiometry.
  - **Stoichiometric Attributes** (6): Describe the elements present and their relative fractions.
  - **Elemental Properties Attributes** (132): Contain statistics taken over the various elemental properties, weighted by the stoichiometry of the structure.
  - **Attributes based on Valence Orbital Occupation** (4): Depend upon the distribution of valence electrons across different orbitals, i.e. on the total number of valence electrons in each orbital across the structure.
  - **Ionic Character Attributes** (3): Attributes which encode whether the material is ionically bonded.
- **Structural Attributes** (126 total): Attributes which depend on the precise structural configuration, i.e. exactly how the atoms are arranged in space.
  - **Geometry Attributes** (16): Attributes which depend upon the spatial configuration only.
  - **Physical Property Differences Attributes** (110): Contain statistics taken over the differences between elemental properties of neighboring sites in the structure, weighted by the size of the Voronoi cell between the neighbors.

A complete table listing the features is given in table 1. Further details can be found in [27, 29].

Site Statistics	Difference Statistics	Name	Description
1-4	-	Effective Coordination Number	mean, variance, min, max
5-7	-	Mean Bond Length	variance, min, max
8-11	-	Bond Length Variation	mean, variance, min, max
12	-	Cell Volume	Volume of fundamental cell, no statistics
13-15	-	Mean WC Magnitude	shells 1-3, no statistics
16	-	Packing Efficiency	no statistics
133-138	17-21	Atomic Number	
139-144	22-26	Mendeleev Number	
145-150	27-31	Atomic Weight	
151-156	32-36	Melting Temperature	
157-162	37-41	Column	Group in Periodic Table
163-168	42-46	Row	Period in Periodic Table
169-174	47-51	Covalent Radius	
175-180	52-56	Electronegativity	
181-210	57-81	Valence Electron Count	Listed for s,p,d,f orbitals and total
211-240	82-106	Unfilled Count	Number of unfilled orbitals Listed for s,p,d,f orbitals and total
241-246	107-111	Ground State Volume	
247-252	112-116	Ground State Band Gap	
253-258	117-121	Ground State Magnetic Moment	
259-264	122-126	Space Group Number	Index of Space group
127	-	Number of Components	no statistics
128-132	-	$\ell^p$ -norms of Component Fractions	$p \in \{2, 3, 5, 7, 10\}$
265-268	-	Fraction of Valence Electrons in s,p,d,f orbitals	no statistics
269	-	Can Form Ionic Compound	boolean, no statistics
270-271	-	Ionic Character	max, mean over pairs of species

Table 1: List of Features with Descriptions. **Site Statistics** refers the mean, range, standard deviation, maximum, minimum, and mode unless otherwise stated in the description. **Difference Statistics** refers to the mean, variance, minimum, maximum and range of the differences between neighboring sites in a structure, weighted by the size of the face between them in the Voronoi tessellation.

## 2.2 Machine Learning Techniques Overview

The class of deep learning methods have been remarkably successful in recent years in applications ranging from computer vision to natural language processing and simulations of quantum systems [33–36]. Although deep neural networks have existed for a long time [37], and had been successfully applied to computer vision tasks [38–40], a major breakthrough was the AlexNet network [41], which dramatically improved the accuracy achievable on large-scale image classification. Following this success, deep neural networks have been very intensively studied and applied to a variety of problems [33–35]. Deep neural networks are particularly effective when applied to regression problems, where one is learning a functional relationship between a feature and a prediction. For many problems, deep neural networks are able to achieve significantly better performance than competing machine learning meth-

ods, due to their ability to learn more complex relationships. With materials science being a field where many complex dependencies are intertwined, it is to be expected that this superior pattern recognition can carry over to the improvement in prediction of material properties.

### 2.2.1 Regression Problem Formulation

The general formulation of a regression problem in statistical machine learning is to find a function  $f : X \rightarrow Y$  which minimizes the risk [42], also known as loss or expected error.

$$R(f) = \mathbb{E}_{x,y \sim \mathcal{P}} l(y, f(x)). \quad (1)$$

Here  $X$  denotes a space of input features,  $Y$  denotes an output space, the expectation above is taken over an unknown distribution  $\mathcal{P}$  on  $X \times Y$  (representing the true relationship between inputs and outputs), and  $l$  is a given loss function. The goal is to find a function  $f$  which accurately predicts the (potentially random) output  $y$  given an input  $x$ .

In this work,  $x \in X$  represents the input features (descriptor) characteristic of the material, and  $y \in Y$  represents the formation energy. The distribution  $\mathcal{P}$  represents the true material-property relationship between given descriptor  $x$  and corresponding formation energy. This relation may not be as simple as mapping a given structure to an energy since different DFT methodologies may give different results, based on many variables, such as employed functionals. [43, 44] Consequently it is useful to describe this relationship via a probability distribution. Furthermore, the loss function considered in this paper is the commonly used  $\ell^1$  or absolute error (AE) loss function  $l(y_1, y_2) = |y_1 - y_2|$ .

In practice, the distribution  $\mathcal{P}$  is not known. Indeed it is this relationship that one is trying to learn in the first place. Instead, what is available is data  $\{(y_i, x_i)\}_{i=1}^n$ , which is sampled from  $\mathcal{P}$ . From this one forms the empirical risk [45, 46]

$$L(f) = \frac{1}{n} \sum_{i=1}^n l(y_i, f(x_i)), \quad (2)$$

and seeks a function  $f$  which minimizes the empirical risk, also known as the training error.

In addition, one must specify the type of relationship that is expected to be found between the inputs  $x_i \in X$  and the predictions  $y_i \in Y$ . This is done by restricting the function  $f$  to a specific class. For instance, by restricting  $f$  to be linear, which corresponds to looking for a linear relationship between  $x_i$  and  $y_i$ , one obtains a linear regression. On the other hand, choosing  $\mathcal{F}$  to be a reproducing kernel Hilbert space of functions on  $X$  with the same loss  $l$  one obtains the kernel ridge regression method. Thus in order to fit the model, the training error is minimized over a specific class of function  $\mathcal{F}$ , i.e. one solves the optimization problem

$$f^* = \arg \min_{f \in \mathcal{F}} L(f) = \arg \min_{f \in \mathcal{F}} \frac{1}{n} \sum_{i=1}^n l(y_i, f(x_i)). \quad (3)$$

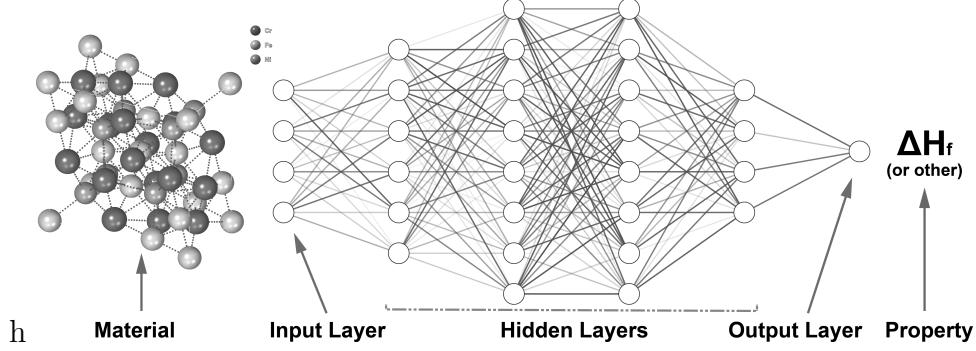


Figure 2.1: Simplified artificial neural network schematic

### 2.2.2 Artificial Neural Networks

In this the class of functions  $\mathcal{F}$  is chosen as the set of functions defined by a neural network architecture (schematic in Figure 2.1), which leads to a deep learning method. A neural network architecture consists of a sequence of alternating linear functions and point-wise non-linear functions [47]. In the figure 2.1 the nodes, or neurons, represent applications of a point-wise non-linear function, called an activation function, and the connections between nodes represent linear functions from the output of the nodes in one layer to the input of the next layer.

The class of functions represented by the neural network consists of the functions obtained by substituting different linear maps between each layer. Specifically, given weight matrices  $W_1, \dots, W_n$  and biases  $b_1, \dots, b_n$ , which are parameters of the network, the corresponding neural network function is given by the composition

$$f_{W_1, \dots, W_n, b_1, \dots, b_n}(x) = W_n \cdots \sigma(W_3 \sigma(W_2 \sigma(W_1 x + b_1) + b_2) + b_3) \cdots + b_n \quad (4)$$

where  $\sigma$ , called the activation function, is applied pointwise to each entry of the vector input (previous layer output). The neural network architecture is determined by the type, dimensionality, activation function  $\sigma$ , and arrangement of intermediate layers. This can potentially introduce some additional restrictions on the linear maps  $W_i$ , see for instance convolutional neural networks, where the linear maps  $W_i$  are restricted to be convolutions with small kernels [38, 40, 41]. The activation functions which we tested in this work include the softsign [48], logistic sigmoid, rectified linear unit [49], and exponential linear unit [50]. Plots of these activation functions can be found in figure 2.2.

Once the neural network architecture has been set, one must fit the values of the parameters  $W_1, \dots, W_n$  and  $b_1, \dots, b_n$  by optimizing the training loss  $L$ ,

$$\arg \min_{W_1, \dots, W_n, b_1, \dots, b_n} L(f_{W_1, \dots, W_n, b_1, \dots, b_n}). \quad (5)$$

This optimization problem is typically solved using stochastic gradient descent [40], or a more robust method such as ADAM [51], which was used in the present work. To solve

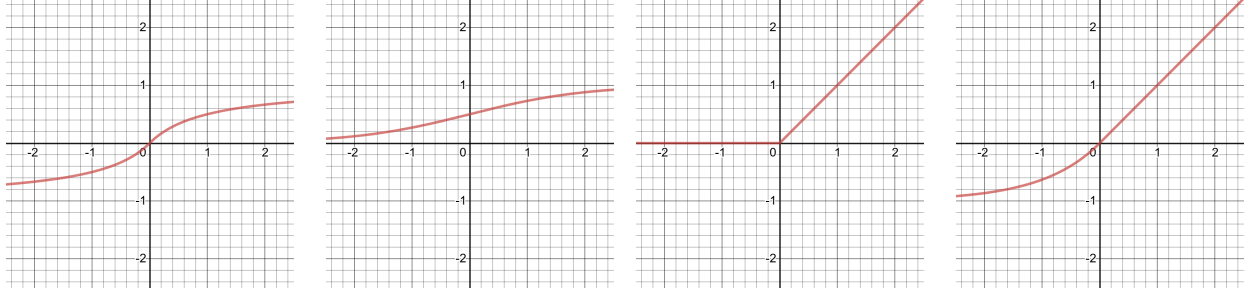


Figure 2.2: Activation functions, from left to right: Soft-sign, logistic sigmoid, exponential linear unit (ELU), and rectified linear unit (ReLU).

the problem faster and to mitigate overfitting, which is discussed in the next sections, these methods form an estimate of the loss function gradient by considering a small subset of the data, called a batch. The batch  $B$  is used to adjust the parameters  $\theta = W_1, \dots, W_n, b_1, \dots, b_n$  as follows

$$\theta^{new} = \theta^{old} - s \nabla_{\theta} \left( \sum_{(x,y) \in B} l(y, f_{\theta}(x)) \right), \quad (6)$$

where  $s$  is the learning rate (the decay rate of the loss function) which can be changed throughout the training, to avoid issues such as gradient explosion, or being stuck in local minima for substantial time. Importantly, the above sum is over all of the data in the batch, so parameters ( $w$  and  $b$ ) are updated based on many datapoints, rather than a single one. Most of models created in the present work used a batch size of 2,048 datapoints.

This methodology has been successfully applied to a variety of practical machine learning problems [41, 52, 53]. Specifically relevant to this work, neural networks have been applied to problems in computational materials science [54, 55]. For example, in [54] neural networks are used to classify the phases of high-entropy alloys. For this application, their neural network models compare favorably to other machine learning algorithms such as  $k$ -nearest neighbor (KNN) and support vector machines (SVM).

Furthermore, in [55] it is shown that even when training on small datasets which are typical of certain materials science problems, specifically in the prediction of solidification defects from optical microscopy data, deep neural networks can achieve better performance than other machine learning models. This is enabled by using a stacked auto-encoder (shallow neural network) to pre-train the deep neural network, whose weights are then fine-tuned on the small dataset. This work complements these studies by applying deep neural networks to the prediction of thermodynamic quantities from atomic structure descriptors.

### 2.2.3 Overfitting

A major problem in statistical learning is avoiding overfitting [45], which, in simple terms, signifies that the model memorizes the training data instead of learning the true relationship



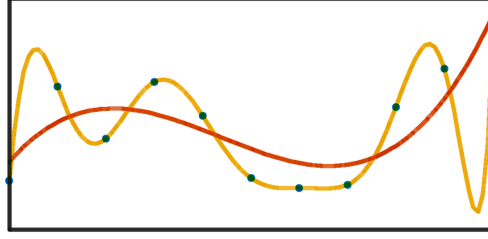


Figure 2.3: A schematic of overfitting. The overfit model is too complex and memorizes the training data. This results in very low training error, but also very poor performance when predicting new data (test error).

between descriptors  $x$  and predictions  $y$ . This occurs when the class of functions  $\mathcal{F}$  is too large, and at the optimal function  $f^*$  in (3) the empirical (2) and true risk (1) diverge sharply. This results in very low training error, but poor performance on data that was not presented to the network.

Overfitting is typically detected by separating the training data into two sets, the data used in (3) to learn the function  $f^*$ , called the training data, and a separate set of data used to evaluate the performance of  $f^*$ , called the validation set. Consequently, in addition to the training loss in (3), the validation error

$$L_{val} = \frac{1}{m} \sum_{i=1}^m l(\tilde{y}_i, f(\tilde{x}_i)), \quad (7)$$

where  $(\tilde{y}_i, \tilde{x}_i)$  for  $i = 1, \dots, m$  is the validation set, which was not presented to the network when adjusting its parameters, is used to detect overfitting. The fraction of the data set aside for validation set should be large enough to be representative of the whole dataset to provide statistically significant conclusions, yet small enough so that knowledge loss in the process is minimized. In this work, a randomly selected 15% of every dataset has been used as validation sets for all training. This corresponded to 65,300 datapoints in the case of the OQDM dataset described in 2.4.

Typically, the validation loss will be greater than the training loss, as the validation set is not available for training. This is illustrated in Figure 2.4, where the ratio between the validation error (7) and the test error (3) during the course of two trainings of similar NN architectures on the same data with the same learning rate schedule has been plotted. This figure indicates that as the training proceeds, the gap between the training and validation errors widens and then increases. The size of this gap is an estimate measure of how much the model has overfit to the data. In one of the models in this figure extensive techniques to mitigate overfitting have been used (see 2.2.4), and for this model the figure shows that the rate at which the model overfits to the data is much lower. At the same time both model exhibit similar performance on the test set.



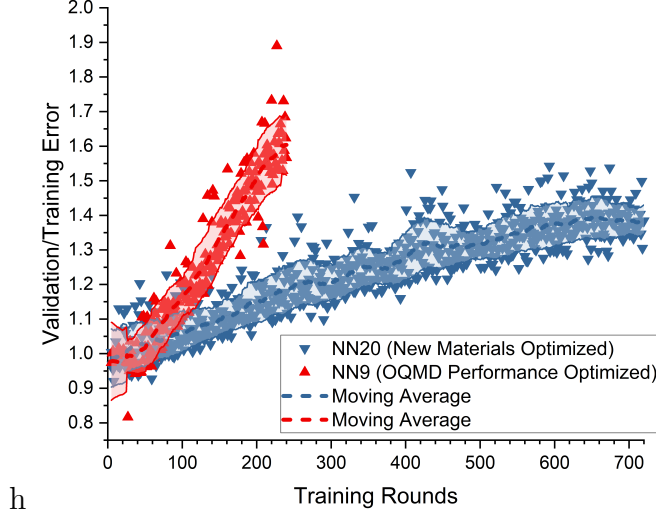


Figure 2.4: Training Loss to Validation Loss in a model that does without (NN9) and with overfitting mitigation (NN20), plotted versus training progress.

#### 2.2.4 Overfitting Mitigation

There are numerous techniques used to prevent the issue of overfitting [45, 56]. These include utilization of a regularization term  $\lambda R(\theta)$  added to the training error (3) to give the regularized empirical loss function

$$f^* = \arg \min_{f \in \mathcal{F}} R_{emp}(f) + \lambda R(\theta). \quad (8)$$

A standard regularizer typically added to the linear regression is the  $\ell^2$ -norm  $R(\theta) = \|\theta\|_2^2$ , which is often called Tikhonov regularization [57] or ridge regression [58]. The  $\ell^2$ -norm is also a popular regularizer in deep learning problems, where it is referred to as weight decay [47]. In the context of this work, it is implemented as a part of the training process, rather than network architecture, and causes rejection of some features in the descriptor that are not contributing to pattern recognition. Results of its implementation are shown throughout Section 2.5.

Another important method used to prevent overfitting in machine learning is the Dropout technique [59]. The concept behind Dropout is to prevent neurons in the network from becoming overly dependent on the output from specific neuron in the previous layer, often referred to as hard-wiring neuron paths. A Dropout layer, placed within a neural network, is implemented as a function operating during the training process and randomly discarding a specified fraction  $p$  of previous layer outputs and multiplying the remaining values by  $1/(1 - p)$ . This forces the pattern recognition ability to be dispersed across the network, as during evaluation of every training step, a random part of the network is acting as if it was not gone. Once the training is completed, all Dropout layers are deactivated and simply pass all information forward, so that the model returns to its deterministic character.

In the experiments performed in this work, as later discussed in 2.5, both Dropout and

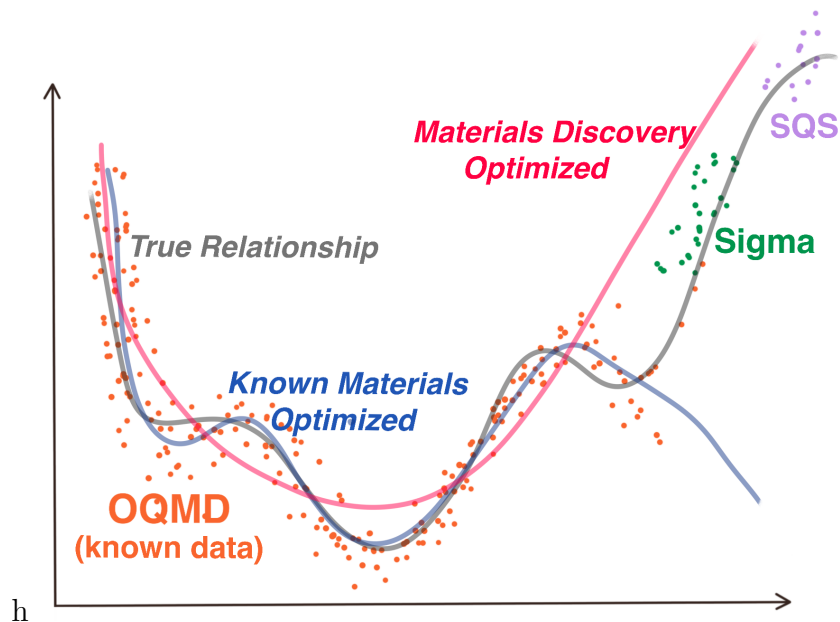


Figure 2.5: A conceptual drawing depicting how overfitting mitigation effort can improve performance beyond regions with high known data density.

weight decay were used to mitigate overfitting, with good effects shown in in particular in Figure 2.4.

Methods for avoiding overfitting typically come with one or more "hyperparameters" (i.e. parameters which control the training process) that can represent how much confidence is given to the training data versus prior knowledge. For instance, if a regularizer is used, the strength of the regularizer,  $\lambda$ , would be a hyperparameter. In the terms of this work, it generally corresponds to how many features in the material descriptor can be considered non-essential to making predictions and therefore discarded systematically throughout the training. Furthermore, when using Dropout, the probability  $p$  is also a hyperparameter.

One typically trains the model on the training dataset using a number of different hyperparameters and then subsequently chooses the best set of them using the validation error. This allows the determination of hyperparameter values which are appropriate to the problem at hand. However, in order to ensure that the determined hyperparameter values are not overly specific to the validation set, the final accuracy of the model is evaluated on a test set which was not used at all during training [45].

Additional advantage of mitigating overfitting to known data can be increased performance during extrapolation, as depicted conceptually in Figure 2.5. This is thanks to reduced model complexity, that forces recognition of stronger and more broadly exhibited patterns rather than small deviations present in the training data, whether real or due to noise, that can significantly degrade extrapolation capability of the ML model. It is important to recognize that cost of such such model simplification is often reduced performance on previously unseen data that lays within the known region.

### 2.2.5 Transfer Learning

Finally, one should consider the technique of transfer learning, which has been observed among deep learning models across a variety of domains [60–63]. Transfer learning refers to the ability of properly trained deep learning models to ‘transfer’ their knowledge to related tasks. In the least complex approach, one does this by simply ‘fine-tuning’ the parameters of the model using new training data (from the new task). This has to be done using a small learning rate and a small number of iterations on a loss function defined by the new training data. It has been observed that this often produces accurate results on the new task for a relatively small amount of additional data.

As an illustrative example, in [61], a network is first trained to recognize lower case handwritten characters. It is then shown that with minimal ‘fine-tuning,’ such a network can be made accurately recognize upper case characters. The same phenomenon was also observed with a network which was first trained to recognize Chinese characters. Considering that this behavior has been widely observed [60, 62, 63], this shows that deep neural networks are often able to transfer knowledge between different but related tasks.

This work adds to this evidence by showing that a network trained on the knowledge from OQMD database covering a broad yet limited spectrum of material, can be easily adjusted to materials outside this spectrum with very little cost relative to the initial training. Specifically, the set of all (243) Fe-Ni-Cr  $\sigma$ -phase endmembers, described in 2.4, is shown in 3.4 to require transfer of only a few examples from that set to dramatically improve model performance on the rest.

## 2.3 Software Used

The choice of software for the machine learning portion of this project was Apache MXNet. [64] Adopting this framework allowed great scalability, as the same code could be used to perform neural network training on a laptop with low-power CPU/GPU and a supercomputer (ORNL Summit) with hundreds of powerful GPU’s. It also allowed portability, since trained nets can be converted and used with other popular frameworks like Google Tensorflow, Pythorch, or even Apple Core ML.

MXNet was accessed through the Wolfram and Python languages. Wolfram Language was used primarily for the network architecture design, training, and testing, as it provides an excellent front-end with detailed training results shown in real-time during the training process. It also provides superior out-of-the-box performance due to its well optimized memory handling when training on a single GPU setup.

Python, on the other hand, was used when writing the end-user tool for running previously trained networks. This choice was made so that the software is completely open-source and can be easily modified for specific purposes or incorporated within other packages. Furthermore, Python allowed quick implementation of a Graphical User Interface (GUI) through the wxpython package.

## 2.4 Data Acquisition and Curation

Four sets of data were used within this work. The largest by volume and significance was the Open Quantum Materials Database (OQMD) [1,2], which contains the results of Density Functional Theory (DFT) calculations performed by the Vienna Ab Initio Simulation Package (VASP) [65] for a broad spectrum of materials. The snapshot used here was extracted from the database by Ward et al. in 2017 and contained 435,792 unique compounds [29]. The second database was a part of the Inorganic Crystal Structure Database (ICSD), a subset of the OQMD with only experimentally-tested structures containing over 30,000 entries. It was extracted at the same time as the OQMD. These two databases were used for both training of the predictive models and later for testing them. ICSD was primarily used for simple neural network architectures at the beginning, and OQMD used for more complex models designed later.

Two smaller data sets were used, in addition to these large databases. The first small dataset contained DFT-calculated formation energies of Fe-Cr-Ni ternary  $\sigma$ -phase endmembers in the 5-sublattice model [66]. As this model contains 5 chemically distinct positions (Wyckoff positions), populated by one of 3 elements, in total it included 243 ( $3^5$ ) structures with 30-atom bases each. This data served as an example of a relatively complex structure that was not included in the OQMD and was not similar to any existing entry. Furthermore, it was a test case of a material that is highly industry-relevant, as it causes steel embrittlement [67] and is costly to investigate using traditional methods due to compositional and configurational complexity. The second small dataset included 13 Special Quasirandom Structures (SQS), which are best periodic supercell approximations to the true disordered state of metal alloys. [68–70] SQS structures in this set were binary alloys containing Fe, Ni, Co, and V, laying on deformed FCC (A1), BCC (A2), or HCP (A3) lattices. They are listed in the supplement to this article. The main purpose of this dataset was to test the performance of the model on a disordered structure that, like Fe-Cr-Ni  $\sigma$ -phase, was not a part of the training set.

Throughout the network design process described in 2.5, it was found that a small fraction of the OQMD dataset (under 0.03%) contains values of formation energy above 10 eV/atom. In the extreme case of  $CuO_2$  (OQMD ID: 647358) this value was 1123 eV/atom or 108350 kJ/mole. Since the source database contains hundreds of thousands of datapoints reported by many scientists, it can be expected that a small fraction of the data may contain some sort of errors and in the present work they were removed from the all datasets used for training and evaluation.

## 2.5 Neural Network Design Process and Intermediate Results

The neural network design process was conducted in incremental fashion, starting from a perceptron, which is the simplest type of neural network proposed by Frank Rosenblatt in 1957 [71]. It effectively operates as a linear function  $f(\vec{d}) = A(w_1d_1 + w_2d_2 + \dots + w_nd_n)$  where  $d_i$  is  $i$ -th element of the descriptor  $\vec{d}$ ,  $w_i$  is the weight associated with it, and  $A$  is an activation function that can introduce non-linearity or turn it into a classifier. Here, the

popular Sigmoid activation function was used.

The perceptron was first trained on the data from the first 5000 entries in the ICSD, to check whether the training was set up correctly. It achieved a MAE of 195 meV/atom on the test set of 230 randomly selected entries ( $\approx 5\%$  from 5000). Results are shown in Figure 2.6.

When trained on the data from all entries in the ICSD, it achieved a MAE of 364 meV/atom on the test set ( $\approx 5\%$  from 32116). This error is comparable to the performance of a random-forest model based on PRDF (370 meV/atom), is slightly worse than a CM (250 meV/atom), and is significantly worse than a random-forest model trained on the same descriptor (90 meV/atom), as reported by Ward et al. [29]. Part of the significance of these results is the evident quality of the descriptor, as the model achieved performance that would be considered excellent just a few years prior to the present work, while being much less complex and computationally costly. Furthermore, it is important to note the time- and space-complexity of the perceptron model. Training the final network took less than 8 seconds compared to around 10,000 seconds reported for the aforementioned random-forest methods, and the resulting model occupied less than 1kb of memory. Following the testing of a perceptron, which allowed rough estimation of the a good size of the network (i.e. number of weights), the design of the actual architecture began. All of these steps are schematically depicted in Figure 2.7.

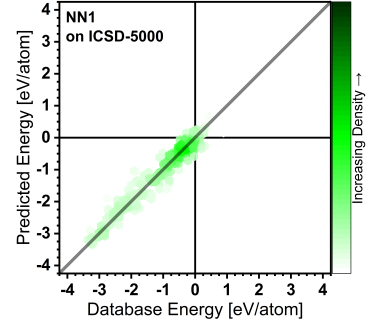


Figure 2.6: Test of perceptron trained on the data from the first 5000 entries in the ICSD dataset and evaluated on the test set of 230 randomly selected entries ( $\approx 5\%$ )

Next, in a few steps, the size of the network was incrementally increased. First, a layer of 1000 neurons was introduced. This reduced the performance on the first 5000 entries in the ICSD, likely due to overfitting issues, as the data was very limited. Performance on the ICSD was improved, reducing the test MAE to 305 meV/atom on the test set, however. Introduction of next two 1000-width layers further reduced the MAE to 215 meV/atom. Based on these results, it was estimated that introducing 4 hidden layers with Sigmoid activation function and widths of 10000, 10000, 1000, and 100 would provide good results when trained on the much larger OQMD.

After switching to OQMD, the network exhibited issues with convergence, often predicting a single value for all of the entries. To mitigate this, the descriptor (i.e. network input) was normalized by dividing every element by its maximum value across the whole dataset. This solved the issue. Next, to improve the training behaviour, the activation functions were changed from only the Sigmoid function to a mix of Soft Sign, Exponential Linear Unit, and Sigmoid, which was found to work well. These steps improved both the predictive performance and reduced the time required to converge. The network architecture resulting from these steps (internally designated NN8 / Simple Good Network in Figure 2.7) was the first to improve performance compared to the Ward et. al approach [29], achieving an MAE of 42 meV/atom on the test set of random subset 5% of OQMD dataset. When testing this

network, a small fraction of around 0.03% of likely incorrect entries in the OQMD were found, as described in 2.4, and were removed from the dataset used later in the design process.

Once a network with desired performance was obtained, the network size was increased until it either exceeded 1GB or showed signs of overfitting. At the first step of this process, two layers of width 10,000 were added, resulting in a network size of 1.2GB and reduced overfitting, as indicated by the ratio of validation-to-training error lowered from 2.2 to 1.6, relative to NN8. The resulting network (internally designated NN9 / OQMD-Optimized Network in Figure 2.7), achieved a MAE of 28 meV/atom on the test set of random subset 5% of OQMD, which was the best performance on OQMD out of all the networks created in this project. Further analysis of the performance is given in 3.2.

Once the main objective of the design process was obtained, i.e. the performance on the OQMD was improved appreciably beyond existing methods, the design process was focused on creating a tool for modeling materials that were not reported in the OQMD. Therefore, the objective changed from achieving the lowest MAE on a random subset 5% of OQMD to: (1) reducing the mismatch between training and validation sets during the training process, (2) keeping the test MAE on the OQMD below 50 meV/atom, and (3) improving performance on two material groups significantly different from the OQMD data, namely Special Quasirandom Structures (SQS) and Fe-Cr-Ni  $\sigma$ -phase (see 2.4).

With these new objectives, two Dropout layers in the middle part of the network were introduced to promote the distribution of pattern recognition abilities across the network. [72] This introduced a problem with convergence as the network became more likely to fall into local minima at the initial stages of the training, which was solved by introducing custom learning rate schedules. Specifically, the learning rate was initially set to a value orders of

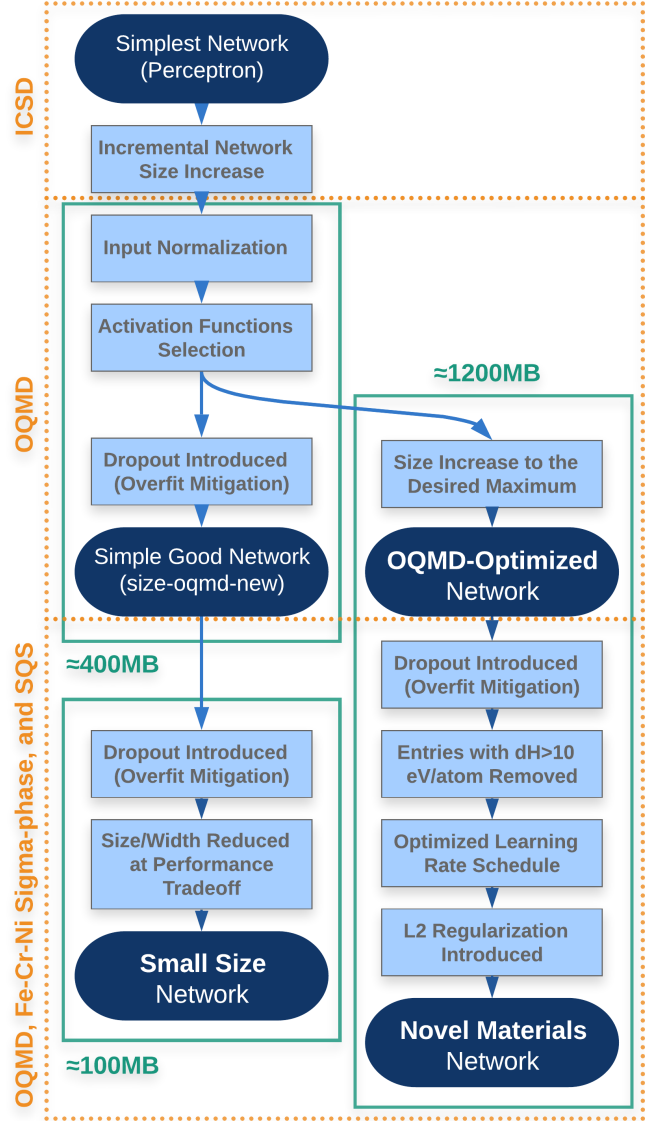


Figure 2.7: The network design process schematic leading to the two final models.



magnitude lower than during the default initial training, and then ramped up to the previous (ADAM default setting in the majority of frameworks) learning rate of 0.001 (or above) after around 2 rounds of training. This type of learning rate schedule is known as warm-up in the deep learning literature [73]. The schedule found to perform the best is presented in Figure 2.8.

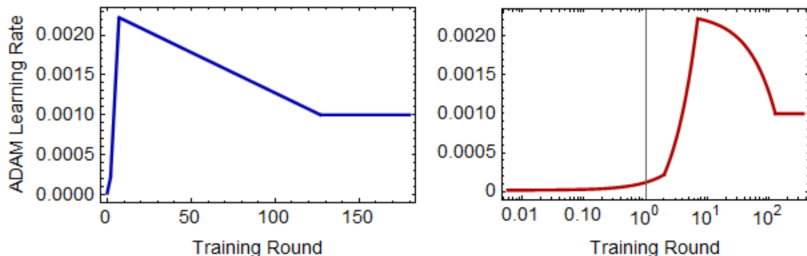


Figure 2.8: The learning rate schedule used for training of networks in the later stage of the design process (NN18). Both left and right plots present the same function, plotted against linear and logarithmic axes respectively.

The next step was the introduction of  $\ell^2$  regularization, which is a technique that favors simplification of the descriptor and effectively rejects features of the descriptor that do not contribute to predictions performance [74]. An overview on it is given in Section 2.2. In the models reported in this work an  $\ell^2$  value of  $10^{-6}$  was used. Higher values were found to stop the training at early stages, impairing the pattern recognition, or in extreme cases (above  $10^{-3}$ ) force the network to discard the input completely, resulting in constant or near-constant output (i.e. mean value from the training dataset predicted for any structure).

The final step was small curation of the training data based on the OQMD-reported structure stability, i.e. the energy difference between the formation energy and the energy convex hull. Motivation for that was the notion that DFT results are inherently less accurate for unstable phases. In this step, all entries with energies of more than 2000 meV/atom above the convex hull were removed from the training set. Importantly, the validation and testing sets were not modified for consistent performance reporting.

All of these changes resulted in a neural network that has been optimized for predicting new materials. In the code and Supplementary materials it is designated as NN20 (Novel Materials Network in Figure 2.7). Compared to the OQMD-optimized network it was derived from, the test MAE on the OQMD increased from 28 to 49 meV/atom. However, at the same time the mismatch between the training and validation set was reduced from 1.57 to 1.38. Or, as presented earlier in Section 2.2.4 in Figure 2.4, reduced to about 1.15 for the same training duration. Furthermore, a relatively large portion of this error can be attributed to some unstable structures that were removed from the training set, but not from test set. Once entries with formation energies of more than 1000 meV/atom above the convex hull were removed, the test MAE decreased to only 38 meV/atom. Restricting the test set further to only somewhat stable structures (stability below 250 meV/atom) resulted in MAE of 30 meV/atom.

While the new-material-optimized network presented an increased MAE across a random

subset of the OQMD, performance has significantly improved on the Fe-Cr-Ni  $\sigma$ -phase described in 2.4. The MAE has decreased from 55 to 41 meV/atom, indicating that the model based on this neural network is more capable of making predictions for new materials.

Once two performance-oriented models were developed, increasing the performance-to-cost ratio has been explored with the motivation that some studies would benefit from many times higher throughput at minor accuracy decrease. Architecture design started from selection of a network with balanced size-to-performance ratio (NN8) and introduction of overfitting mitigation technique (Dropout [59]) used for the network optimized for new materials, as depicted in Figure 2.5. Next, the network was gradually narrowed (less neurons in layers) until the performance started to noticeably deteriorate (41.9 meV/atom for 5000- and 4000-width vs 42.1 for 3000-width). This approach allowed significant reduction of the network size (and the computational intensity to run it) from around 1,200MB to around 145MB. If an application demands even more of a reduction in model size and computational cost, the same procedure could be continued until some minimum required performance is retained.

## 3 Results

### 3.1 Final Predictive Models

Throughout the extensive architecture design process detailed in 2.5 and depicted in Figure 2.7, new network architectures were designed and tested in various ways, leading to about 50 predictive models (trained neural networks) with varying training parameters and training data. The majority of the intermediate networks were recorded and stored for the record, and are available upon request.

Input	vector (size: 271)	Input	vector (size: 271)	Input	vector (size: 271)
1 LinearLayer	vector (size: 10000)	1 LinearLayer	vector (size: 10000)	1 LinearLayer	vector (size: 4000)
2 SoftSign[x]	vector (size: 10000)	2 SoftSign[x]	vector (size: 10000)	2 SoftSign[x]	vector (size: 4000)
3 LinearLayer	vector (size: 10000)	3 DropoutLayer	vector (size: 10000)	3 DropoutLayer	vector (size: 4000)
4 LogisticSigmoid	vector (size: 10000)	4 LinearLayer	vector (size: 10000)	4 LinearLayer	vector (size: 4000)
5 LinearLayer	vector (size: 10000)	5 LogisticSigmoid	vector (size: 10000)	5 LogisticSigmoid	vector (size: 4000)
6 LogisticSigmoid	vector (size: 10000)	6 DropoutLayer	vector (size: 10000)	6 DropoutLayer	vector (size: 4000)
7 LinearLayer	vector (size: 10000)	7 LinearLayer	vector (size: 10000)	7 LinearLayer	vector (size: 4000)
8 LogisticSigmoid	vector (size: 10000)	8 ExponentialLinearUnit[x]	vector (size: 10000)	8 ExponentialLinearUnit[x]	vector (size: 4000)
9 LinearLayer	vector (size: 1000)	9 DropoutLayer	vector (size: 10000)	9 DropoutLayer	vector (size: 4000)
10 ExponentialLinearUnit[x]	vector (size: 1000)	10 LinearLayer	vector (size: 10000)	10 LinearLayer	vector (size: 1000)
11 LinearLayer	vector (size: 100)	11 LogisticSigmoid	vector (size: 10000)	11 ExponentialLinearUnit[x]	vector (size: 1000)
12 ExponentialLinearUnit[x]	vector (size: 100)	12 DropoutLayer	vector (size: 10000)	12 DropoutLayer	vector (size: 1000)
13 LinearLayer	vector (size: 1)	13 LinearLayer	vector (size: 1000)	13 LinearLayer	vector (size: 100)
Output	vector (size: 1)	14 ExponentialLinearUnit[x]	vector (size: 1000)	14 ExponentialLinearUnit[x]	vector (size: 100)
		15 DropoutLayer	vector (size: 1000)	15 LinearLayer	vector (size: 1)
		16 LinearLayer	vector (size: 100)	Output	vector (size: 1)
		17 ExponentialLinearUnit[x]	vector (size: 100)		
		18 LinearLayer	vector (size: 1)		
		Output	vector (size: 1)		

Figure 3.1: Three selected architectures designed within this work. Optimized for: (Left) OQMD performance, (Middle) predicting new materials, (Right) small size at good performance. Internally in the code, they are designated as NN9, NN20, and NN24.



Out of all trained neural networks, three were selected and can be considered final outcomes of the design process, optimized for different objectives. Their architectures are presented in Figure 3.1.

The first one, denoted NN9, was created specifically for the OQMD performance. This was the same objective as in the study by Ward et al. [29], which was a direct inspiration of this work. The performance of this network serves as a direct comparison to the Random Forest method employed in that paper [29] and other works [30, 31].

The second network was optimized for improved pattern recognition on OQMD and improved performance on non-OQMD datasets used in the present work (i.e. SQS/ $\sigma$ -phase datasets). This was achieved primarily through extensive overfitting mitigation which lead to a network with improved materials-discovery capability. Furthermore, these overfitting mitigation methods, in particular the regularization described in 2.2.4, have allowed identification of descriptor attributes that contributed the most to the predictive capability and the ones that were almost completely discarded once penalty for considering them was assigned. Figure 3.2 presents the distribution of sums of squared weights between each neuron in the input (each of the 273 features in the descriptor) and all 10,000 neurons in the first hidden layer (Figure 2.1 offers visual aid to the concept).

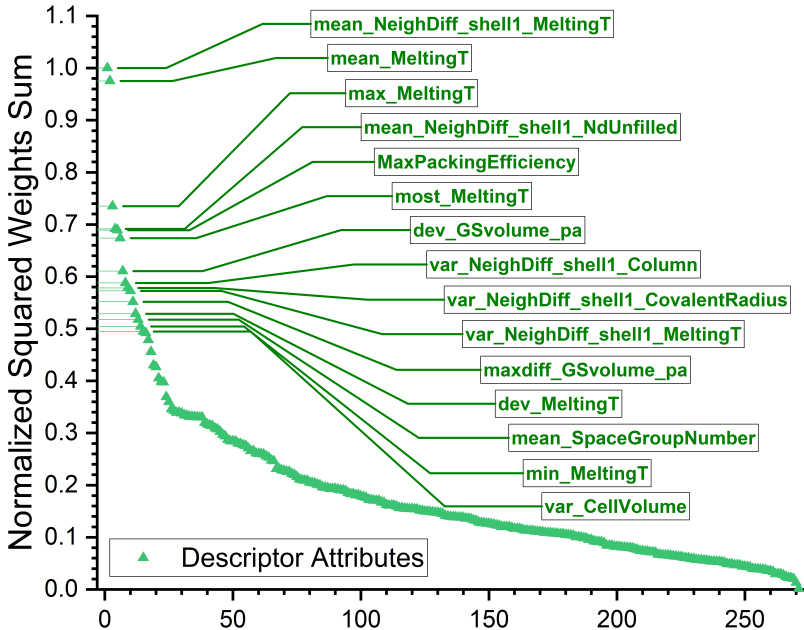


Figure 3.2: The distribution of sums of squared input weights. High values correspond to attributes that were not lowered due to their contribution to pattern recognition of the model. 15 attributes with the highest values are labeled.

The third, smallest network, denoted NN24, was created for memory/power constrained applications requiring a balance between OQMD performance and memory-intensity and processing power required. Model parameters contained in this architecture occupy only 145MB, over 8 times less than two other models and around 200 times less than model reported by Ward et al. [29].

Details regarding hyper-parameters and training routines used to obtain three resulting models can be found in the Supplementary Materials.

### 3.2 OQMD Data Performance

As described in 2.5, all three final networks were evaluated on a randomly selected subset of the OQMD to give a comparison between the state-of-the-art model presented by Ward et al. [29] and the redesigned machine learning method presented here. This random subset consisted of 21,800 OQMD entries, constituting approximately 5%, which were not presented to the network, nor used for evaluation at any stage of the training process. This sample size was considered to be representative of the whole dataset once the small fraction (0.026%) of likely incorrect entries were removed from the dataset as described in 2.4. The random selection itself was initially performed separately for each training process and recorded after completion. Later, when networks were modified to mitigate overfitting, a single random subset was used for all of them to allow more careful design and more accurate comparative analysis of results. Figure 3.3 gives (1) prediction vs OQMD values of formation energy plot, (2) statistics related to error in predictions relative to the OQMD values, and (3) a histogram of absolute error in in predictions relative to the OQMD values.

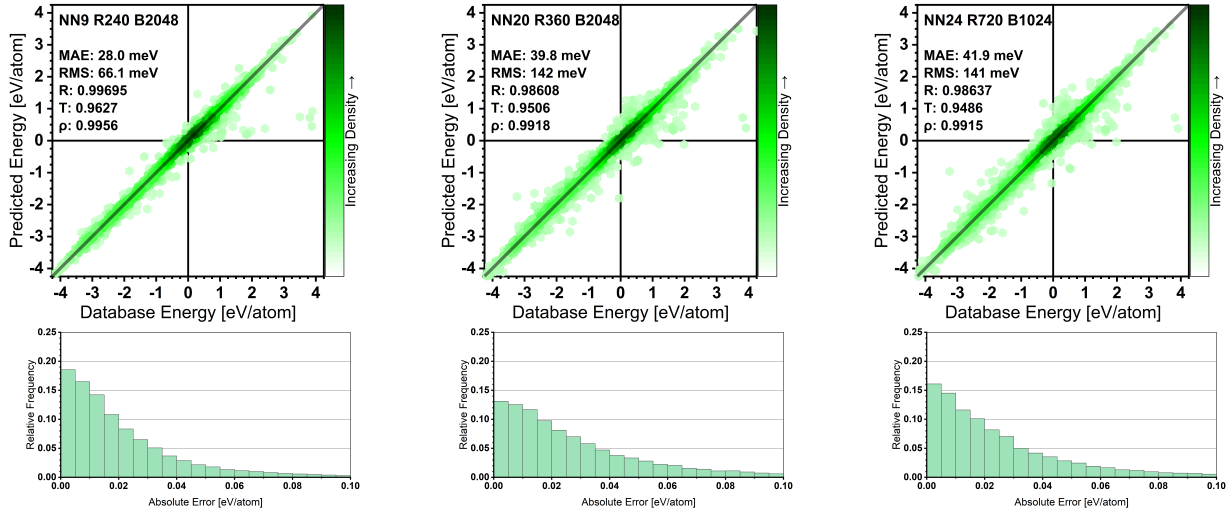


Figure 3.3: Performance of 3 selected neural networks on a random subset of 21,800 entries from OQMD. (Left) OQMD performance, (Middle) predicting new materials, (Right) small size at good performance. Internally in the code, they are designated as NN9, NN20, and NN24.

### 3.3 Non-OQMD Data Performance

Models created in this , specifically the ones optimized for predicting formation energy of new materials, were designed and implemented to serve as tools for materials discovery. Evaluating their performance on data from the same source as the training set done in 3.2

is inherently biased towards favoring models that provide the best fit to the prior (training) knowledge. This is amplified by the fact that many entries in the database are reported in groups that come from a single study and span similar materials, what effectively makes this evaluation more akin to interpolation than extrapolation of knowledge.

To partially mitigate the described issue, the performance of the models was also evaluated on two smaller non-OQMD databases that were not presented to the network in any capacity during the training process, nor were similar entries shown. In all cases, models created in this paper were able to achieve approximately the same performance as on a random selection from the OQMD. To give a perspective, Figure 3.4 shows predicted and database values of formation energy against the same axis as the top row in Figure 3.3.

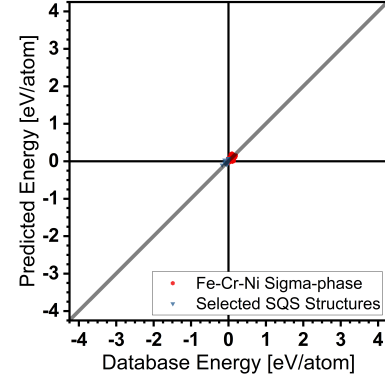


Figure 3.4: Predictions of formation energy using the new-materials=optimized network (NN20) evaluated on (red) Fe-Cr-Ni  $\sigma$ -phase, and (blue) SQS structures. Compare to Figure 3.3 with the same axis for OQMD data.

As shown, the model was able to give rather accurate predictions relative to the random subset of the OQMD. To give a more in-depth analysis of the results, Figure 3.5 shows a magnified view of the predictions and basic statistics on the agreement between predictions and database for the three models developed in this work.

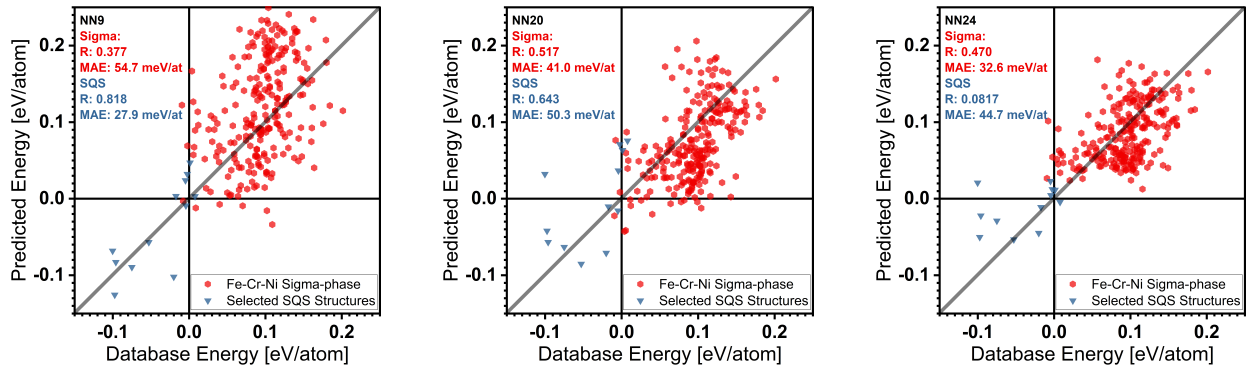


Figure 3.5: Performance of 3 selected neural networks on non-OQMD data described in 2.4. Evaluated on (red) Fe-Cr-Ni  $\sigma$ -phase and (blue) SQS dataset. Networks organized by columns; optimized for (left) OQMD performance, (middle) predicting new materials, (right) size-constrained applications. Internally in the code, they are designated as NN9, NN20, and NN24 respectively.

While all three models performed at around the same MAE level as for the OQMD, it is clear that the network optimized for new materials performed the best on both test cases. It provided major increases in the Spearman Rho and Kendall Tau correlations. The Pearson correlation slightly decreased in the first case and slightly increased in the second case.

In both cases, the mean average error decreased by about 20% compared to the OQMD-optimized model.

### 3.4 Transfer Learning Capability

As mentioned earlier in this, ML models such as the ones used by SIFFENN can be used to transfer knowledge from one problem to a related one. While there are numerous possible applications, within this paper one most commonly used implementation of transfer learning was implemented. Namely, that the model can be easily adopted to a new material system it wasn't trained on through the transfer learning from OQMD and very sparse information from a new system. Such a problem is analogous to many others in materials science, where general knowledge is used to make meaningful statements without statistically significant patterns in locally available data.

In a test implementation of such a process done here, the ML model was first trained on a broad and general material dataset (OQMD) and then further trained (re-trained) for a given number of rounds on the new data (Fe-Ni-Cr  $\sigma$ -phase dataset), at a much smaller learning rate. This allowed the model to adapt to the new system, while still conserving its broad knowledge, and can be thought as fine tuning a model to improve extrapolation outside of a prior knowledge space.

In order to achieve good performance, both number of rounds and learning rate have to be optimized. This can be accomplished by investigating dependence of error on fraction of available data while one of these parameters is fixed. Figure 3.6 presents the dependence of transfer learning from new data for different learning rates expressed as fractions of default ADAM learning rate (0.001 shared across a vast majority of software).

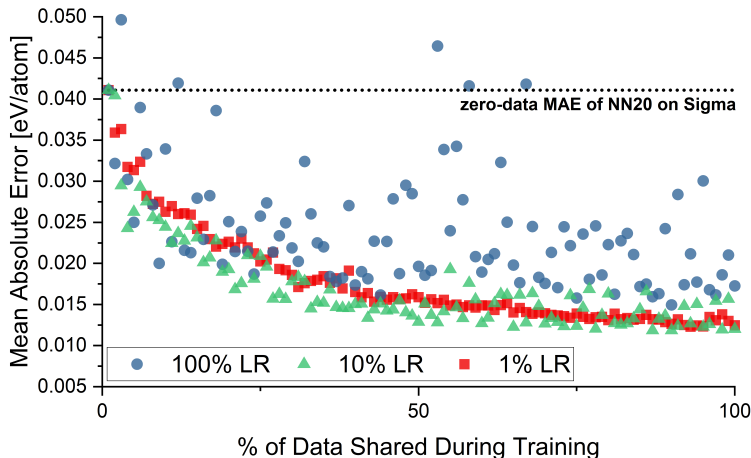


Figure 3.6: MAE evolution of NN20 model re-trained for 25 additional rounds (times each example is evaluated) on an increasing fraction of data from Fe-Cr-Ni  $\sigma$ -dataset. Presents the dependence of transfer learning from new data for different learning rates expressed as fractions of default ADAM learning rate found in the majority of machine learning software.

As shown, in this case, the default learning rate cannot be used for the transfer learning as it will adjust network parameters in both unreliable and detrimental fashion. The same behaviour would be observed if process were conducted using an automated model design available in software such as Mathematica and MATLAB. The 10% learning rate provided reliable enough outcomes and allowed a better performance improvement given little data, relative to using 1% learning rate. The second parameter to be optimized was the number of re-training rounds, as presented in Figure 3.7.

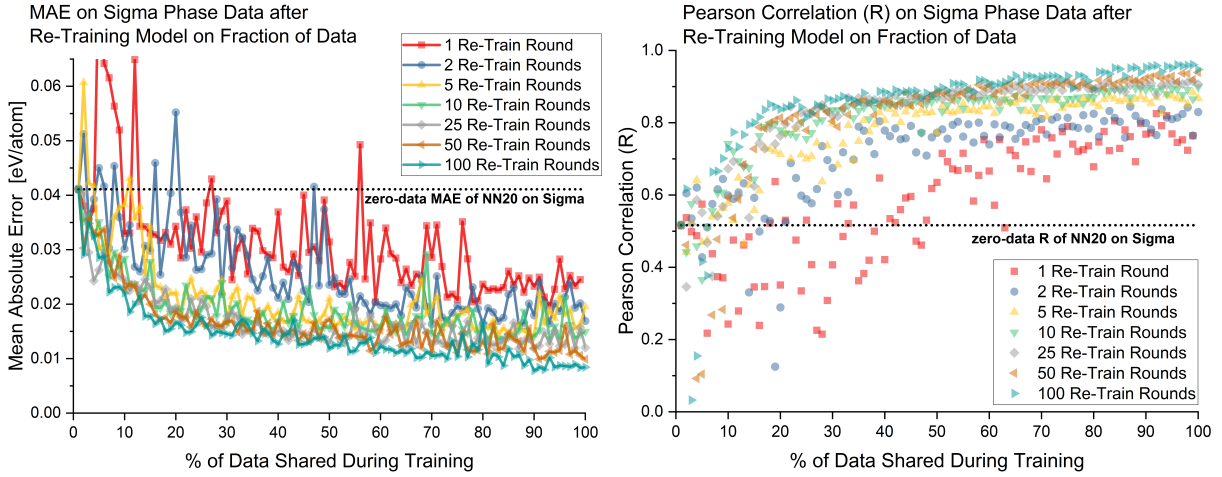


Figure 3.7: MAE and Person correlation (R) evolution of NN20 model re-trained at 10% learning rate on an increasing fraction of data from Fe-Cr-Ni  $\sigma$ -dataset. Presents the dependence of transfer learning from new data for different re-training rounds numbers.

Figure 3.7 shows that too few retraining rounds causes unreliable outcomes, while too many causes overfitting for low amounts of new data. In the case of Fe-Cr-Ni  $\sigma$ -dataset, retraining for 10 or 25 rounds provides balanced results across the whole dataset. With parameters for the process set to 10% learning rate and 25 additional rounds, the performance can be evaluated graphically, as presented in Figure 3.8.

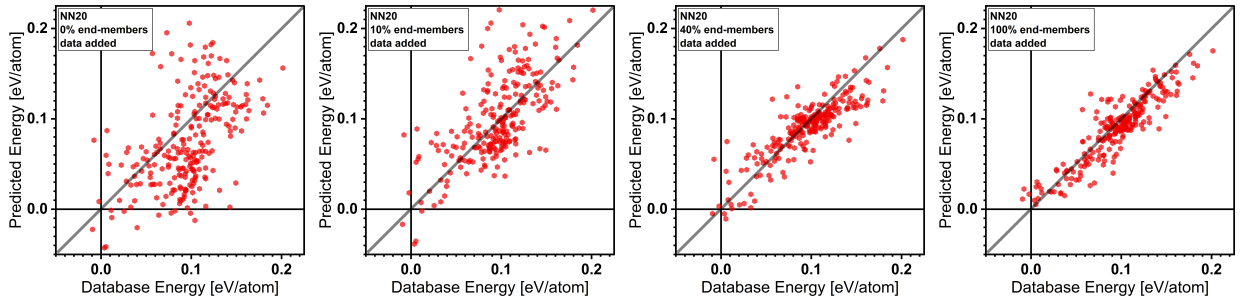


Figure 3.8: Performance of a new-materials-optimized network on  $\sigma$ -phase data. Left-to-right: as trained on the OQMD, with additional training on 10%, 40%, and 100% of the Fe-Cr-Ni  $\sigma$ -phase end-member data. The points on the figure correspond to all end-members (both training and testing data).

As depicted, adding just 10% of DFT-calculated data (24/243 endmembers) provided a significant improvement in the prediction quality over the other 90% that was never shown to the model. This result indicates that the models in this paper can be combined with partial data obtained through DFT calculations to create accurate predictive tools for a specific material system and potentially limit number of calculations required within the study. This can then provide the ability to investigate broader material search spaces at given computational cost.

Furthermore, SIPFENN’s transfer learning capability could be used for a more broad materials exploration without a well defined finite search space like the ternary Fe-Cr-Ni  $\sigma$ -phase. In such case, it is better to evaluate and report the performance of the model on a test set that wasn’t presented during the training and report, as a function of number of added datapoints (new DFT calculations). With such problem statement, the transfer learning process has been repeated 1180 for the statistical significance of the outcomes, which are presented in Figure 3.9.

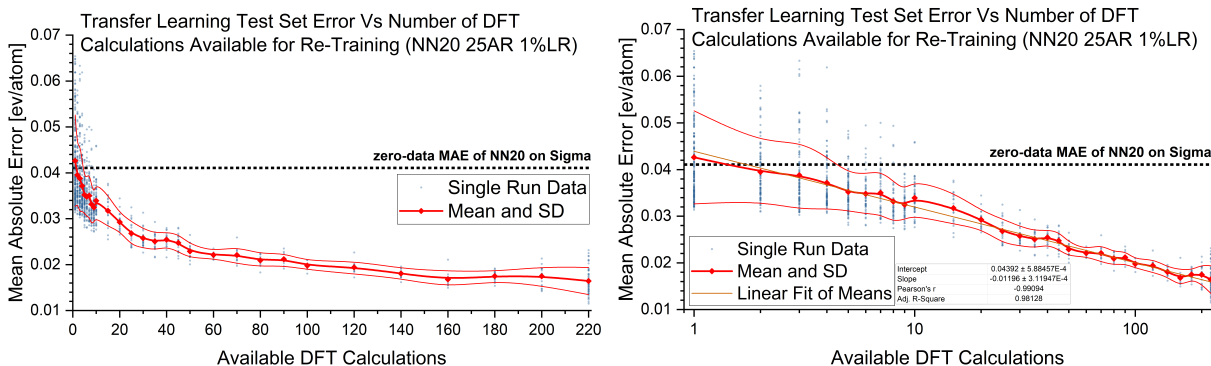


Figure 3.9: MAE of predictions evaluated on test set data vs number of newly available training datapoints. 1180 blue points correspond to single transfer learning processes. Red plot gives mean MAE and standard deviation. Both plots contain the same data.

As presented in Figure 3.9, adding just a small number of new datapoints allows to nearly half the MAE with around 20 datapoints. Furthermore, evident from the right plot, this performance increase is highly predictable following a straight line very well ( $R^2 = 0.98$ ).

### 3.5 End-User Implementation - SIPFENN

One of the objectives of this paper was to create a tool that is transparent, easy to use by the research community, and easily modifiable. This lead to the creation of SIPFENN software. Its name is an acronym for Structure-Informed Prediction of Formation Energy Using Neural Networks. SIPFENN provides the user with near-instant access to the models presented in 3.1. In the future this selection will likely be further expanded. On the user side, the use of the software is as easy as selecting one of the models, specifying a folder containing structure information files like POSCAR [75] or CIF [76], running the predictions, and saving results.



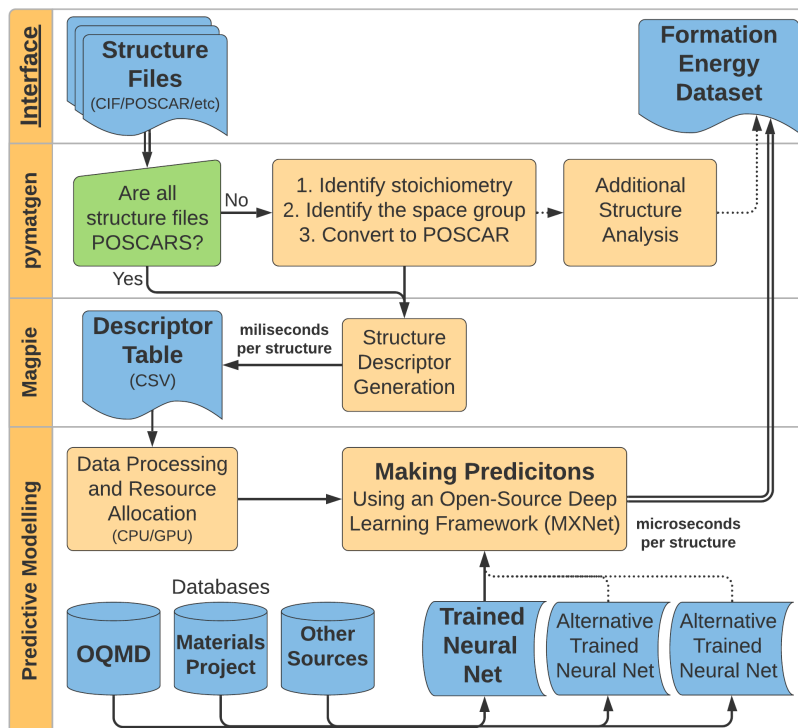


Figure 3.10: SIPFENN schematic description of operation.

SIPFENN was written entirely in Python to allow other researchers to easily modify it and adjust it to specific needs. Its schematic of operation is presented in Figure 3.10. In broad scope, it first performs the structure analysis and modifications using the Python Materials Genomics library (Pymatgen) [77]. In the current implementation, it imports all structure files, analyzes the stoichiometry, creates unique names based on that, and exports them as POSCAR files. This is a rather simple task, however pymatgen is a powerful tool with a suit of more complex analytical tools that can be quickly implemented into SIPFENN by the user with even basic Python skills. Following the analysis, SIPFENN runs java-based Magpie [27] which calculates a descriptor for every imported structure and exports the result as a CSV file. This file is a descriptor table, where each row corresponds to a single material, and which can be stored and re-used later to run multiple predictive models at a fraction of the original computation time. It can also be used to create datasets for training procedures by replacing the last column with calculated or experimental values of formation energy.

Finally, the descriptor table is imported into the MXNet library framework, allocated into the CPU or GPU memory based on user selection, and evaluated using the selected predictive model. Once results are obtained, they are exported in CSV format and can be analyzed by any spreadsheet software such as Microsoft Excel.

SIPFENN was planned as a command line tool, however it was recognized that some users, especially those with little computational background, may find that difficult. Therefore, a simple graphical user interface (GUI) was created using wxPython library. It incorporates all the capabilities of the command line version. Furthermore, it lets the user download the

predictive models from a repository in a single click. A sample snapshot of the GUI before performing calculations is presented in Figure 3.11.

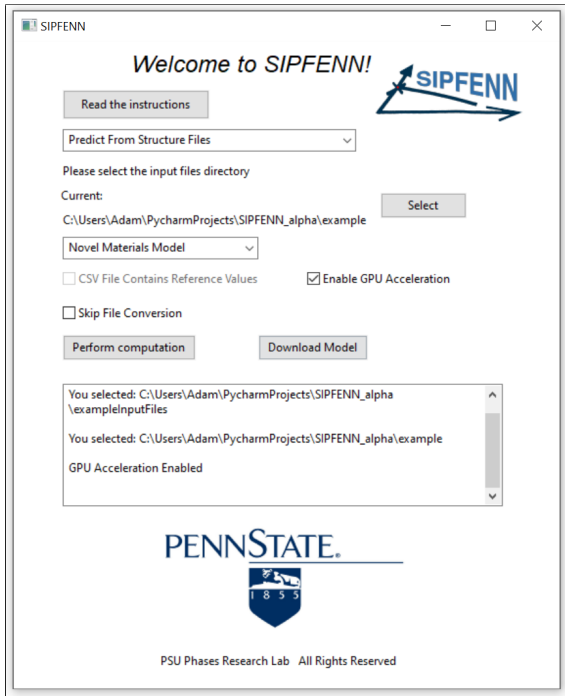


Figure 3.11: A snapshot of the graphical user interface of SIPFENN.

## 4 Conclusions

### 4.1 Summary of Results and Significance

In this paper, based on work done by Ward et al. [29], specifically its dataset and descriptor design, new machine learning models were created, significantly improving both performance and accessibility, through implementation of more robust and much more optimized machine learning techniques. In total, over 50 neural networks were trained on the dataset of around 400,000 DFT calculation results contained within the OQMD database. This process lead to three final neural networks specialized in defined objectives, yet still all having better performance than existing state-of-the-art models on the original objective of achieving the lowest test error. The first network provides state-of-the-art performance on the random subset of OQMD, with mean absolute error (MAE) of 28 meV/atom. The second network provides MAE of 42 meV/atom, which still constitutes a significant improvement over previous tools, but has reduced size, allowing the network to run on low power devices such as smartphones. The third and most advanced neural network was optimized for predicting new materials, and consequently its usability in new materials discovery. In addition to testing models' performance on the OQMD to allow comparison with the current literature data, the three new models were evaluated on two datasets not contained within the OQMD. Performance



on these datasets was found to be equivalent to the one on OQMD, with the model optimized for new materials performing significantly better, even though it was not trained on that new data.

In addition to the neural network design process, it was shown that models created within this paper can be used for transfer learning, where vast knowledge of a broad spectrum of materials is combined with a very limited knowledge of a specific materials system to provide excellent results within that specific system. Such a process mitigates the issue of low data availability, present in numerous materials science problems, and consequently allows users to investigate a broader scope of materials at the same computational cost. In example presented here, providing as little as a few datapoints can provide a significant improvement, decreasing the error by about a factor of two.

Finally, the three neural network models designed within this paper were used, in conjunction with additional software, to create an end-user tool called SIPFENN. SIPFENN’s capabilities extend far beyond allowing validation of the presented results. It is implemented to work without any intensive computations on the user side, to be very fast thanks to using one of the industry’s leading ML frameworks capable of well-optimized computations on GPUs rather than CPUs. Furthermore, it is an open source tool which can be modified to specific needs without an extensive computer science background.

## 4.2 Software Access

The most recent version of SIPFENN code is available through Penn State’s Phases Research Lab website at [www.phaseslab.com/sipfenn](http://www.phaseslab.com/sipfenn) in (1) a minimal version that can be run on pre-computed descriptors in CSV format as well as (2) ready-to use version with pre-compiled Magpie [27]. SIPFENN contains hard coded links to neural networks stored in cloud that can be downloaded at a single-click (see Figure 3.11) or directly from [psu.box.com/v/SIPFENN-NeuralNets](https://psu.box.com/v/SIPFENN-NeuralNets). All neural networks are stored both in (1) open-source MXNet format maintained by Apache Foundation and used within SIPFENN, and in (2) closed-source WLNnet format maintained by Wolfram Research and having advantage of even easier deployment, as well as guaranteed forward compatibility with future versions of Wolfram Language. For further ensured longevity of results, SIPFENN neural networks are also stored at the CERN’s Data Centre through the courtesy of Zenodo.org service under [doi:10.5281/zenodo.4006803](https://doi.org/10.5281/zenodo.4006803).

## 4.3 Acknowledgements

This work was financially supported by the ICDS Seed Grant from the Pennsylvania State University, the Office of Naval Research (ONR) via Contract No. N00014-17-1-2567, the National Science Foundation (NSF) via Grant No. CMMI-1825538, and the Department of Energy (DOE) via Award Nos. DE-FE0031553 and DE-EE0008456.

We would like to thank Zhengqi Liu for his help implementing the graphical user interface, Dr. ShunLi Shang for providing the Fe-Cr-Ni  $\sigma$ -phase dataset, and Brandon Bocklund for providing SQS dataset.

## 5 References

### References

- [1] J. E. Saal, S. Kirklin, M. Aykol, B. Meredig, and C. Wolverton, “Materials design and discovery with high-throughput density functional theory: The open quantum materials database (OQMD),” *JOM*, vol. 65, no. 11, pp. 1501–1509, 11 2013.
- [2] S. Kirklin, J. E. Saal, B. Meredig, A. Thompson, J. W. Doak, M. Aykol, S. Rühl, and C. Wolverton, “The Open Quantum Materials Database (OQMD): assessing the accuracy of DFT formation energies,” 2015. [Online]. Available: [www.oqmd.org/download](http://www.oqmd.org/download).
- [3] A. van de Walle, C. Nataraj, and Z. K. Liu, “The Thermodynamic Database Database,” *Calphad: Computer Coupling of Phase Diagrams and Thermochemistry*, vol. 61, pp. 173–178, 6 2018.
- [4] A. Jain, S. P. Ong, G. Hautier, W. Chen, W. D. Richards, S. Dacek, S. Cholia, D. Gunter, D. Skinner, G. Ceder, and K. A. Persson, “Commentary: The Materials Project: A materials genome approach to accelerating materials innovation,” *APL Materials*, vol. 1, no. 1, p. 011002, 7 2013. [Online]. Available: <http://aip.scitation.org/doi/10.1063/1.4812323>
- [5] S. Curtarolo, W. Setyawan, G. L. W. Hart, M. Jahnatek, R. V. Chepulskii, R. H. Taylor, S. Wang, J. Xue, K. Yang, O. Levy, M. J. Mehl, H. T. Stokes, D. O. Demchenko, and D. Morgan, “AFLOW: an automatic framework for high-throughput materials discovery,” Tech. Rep. [Online]. Available: [www.aflowlib.org](http://www.aflowlib.org)
- [6] C. Toher, C. Oses, D. Hicks, E. Gossett, F. Rose, P. Nath, D. Usanmaz, D. C. Ford, E. Perim, C. E. Calderon, J. J. Plata, Y. Lederer, M. Jahnátek, W. Setyawan, S. Wang, J. Xue, K. Rasch, R. V. Chepulskii, R. H. Taylor, G. Gomez, H. Shi, A. R. Supka, R. Al, R. Al Orabi, P. Gopal, F. T. Cerasoli, L. Liyanage, H. Wang, I. Siloi, L. A. Agapito, C. Nyshadham, G. L. W. Hart, J. Carrete, F. Legrain, N. Mingo, E. Zurek, O. Isayev, A. Tropsha, S. Sanvito, R. M. Hanson, I. Takeuchi, M. J. Mehl, A. N. Kolmogorov, K. Yang, P. D’amico, A. Calzolari, M. Costa, R. De Gennaro, M. B. Nardelli, M. Fornari, O. Levy, and S. Curtarolo, “The AFLOW Fleet for Materials Discovery,” 2018. [Online]. Available: [https://doi.org/10.1007/978-3-319-42913-7\\_63-1](https://doi.org/10.1007/978-3-319-42913-7_63-1)
- [7] G. Pizzi, A. Cepellotti, R. Sabatini, N. Marzari, and B. Kozinsky, “AiiDA: automated interactive infrastructure and database for computational science,” *Computational Materials Science*, vol. 111, pp. 218–230, 1 2016.
- [8] O. Isayev, C. Oses, C. Toher, E. Gossett, S. Curtarolo, and A. Tropsha, “Universal fragment descriptors for predicting properties of inorganic crystals,” *Nature Communications*, vol. 8, 6 2017.

- [9] F. Legrain, J. Carrete, A. Van Roekeghem, S. Curtarolo, and N. Mingo, “How Chemical Composition Alone Can Predict Vibrational Free Energies and Entropies of Solids,” *Chemistry of Materials*, vol. 29, no. 15, pp. 6220–6227, 8 2017.
- [10] G. Pilania and X.-Y. Liu, “Machine learning properties of binary wurtzite superlattices,” *Journal of Materials Science*, vol. 53, 1987. [Online]. Available: <https://doi.org/10.1007/s10853-018-1987-z>
- [11] J. Jung, J. I. Yoon, H. K. Park, J. Y. Kim, and H. S. Kim, “Bayesian approach in predicting mechanical properties of materials: Application to dual phase steels,” *Materials Science and Engineering A*, vol. 743, pp. 382–390, 1 2019.
- [12] B. J. Bucior, N. S. Bobbitt, T. Islamoglu, S. Goswami, A. Gopalan, T. Yildirim, O. K. Farha, N. Bagheri, and R. Q. Snurr, “Energy-based descriptors to rapidly predict hydrogen storage in metal-organic frameworks †,” *Mol. Syst. Des. Eng*, vol. 4, p. 162, 2019.
- [13] A. Chandrasekaran, D. Kamal, R. Batra, C. Kim, L. Chen, and R. Ramprasad, “Solving the electronic structure problem with machine learning,” *npj Computational Materials*, vol. 5, no. 22, 2 2019. [Online]. Available: <https://doi.org/10.1038/s41524-019-0162-7>
- [14] K. Kim, L. Ward, J. He, A. Krishna, A. Agrawal, and C. Wolverton, “Machine-learning-accelerated high-throughput materials screening: Discovery of novel quaternary Heusler compounds Machine Learning Accelerated High-Throughput Materials Screening: Discovery of Novel Quaternary Heusler Compounds,” *Phys. Rev. Materials*, vol. 2, p. 123801, 2018.
- [15] C. Wen, Y. Zhang, C. Wang, D. Xue, Y. Bai, S. Antonov, L. Dai, T. Lookman, and Y. Su, “Machine learning assisted design of high entropy alloys with desired property,” *Acta Materialia*, vol. 170, pp. 109–117, 5 2019.
- [16] L. Scime and J. Beuth, “Using machine learning to identify in-situ melt pool signatures indicative of flaw formation in a laser powder bed fusion additive manufacturing process,” *Additive Manufacturing*, vol. 25, pp. 151–165, 1 2019.
- [17] J. Schmidt, M. R. Marques, S. Botti, and M. A. Marques, “Recent advances and applications of machine learning in solid-state materials science,” *npj Computational Materials*, vol. 5, no. 1, 12 2019. [Online]. Available: <https://www.nature.com/articles/s41524-019-0221-0>
- [18] R. K. Vasudevan, A. Mehta, R. Smith, G. Kusne, F. Tavazza, L. Vlcek, M. Ziatdinov, S. V. Kalinin, and J. Hattrick-Simpers, “Materials science in the artificial intelligence age: high-throughput library generation, machine learning, and a pathway from correlations to the underpinning physics.” [Online]. Available: <https://doi.org/10.1557/mrc.2019.95>
- [19] M. Aykol, V. I. Hegde, L. Hung, S. Suram, P. Herring, C. Wolverton, and J. S. Hummelshøj, “Network analysis of synthesizable materials discovery,”

- Nature Communications*, vol. 10, 2019. [Online]. Available: <https://doi.org/10.1038/s41467-019-10030-5>
- [20] V. I. Hegde, M. Aykol, S. Kirklin, and C. Wolverton, “The phase stability network of all inorganic materials,” *Scientific Advances*, vol. 6, 2020.
  - [21] O. Kononova, H. Huo, t. He, Z. Rong, t. Botari, W. Sun, V. tshitoyan, and G. Ceder, “Text-mined dataset of inorganic materials synthesis recipes,” *Scientific Data*, vol. 6, no. 203, 2019. [Online]. Available: <https://doi.org/10.1038/s41597-019-0224-1>
  - [22] K. Alberi, M. B. Nardelli, A. Zakutayev, L. Mitas, S. Curtarolo, A. Jain, M. Fornari, N. Marzari, I. Takeuchi, M. L. Green, M. Kanatzidis, M. F. Toney, S. Butenko, B. Meredig, S. Lany, U. Kattner, A. Davydov, E. S. Toberer, V. Stevanovic, A. Walsh, N.-G. Park, A. Aspuru-Guzik, D. P. Tabor, J. Nelson, J. Murphy, A. Setlur, J. Grengoire, H. Li, R. Xiao, A. Ludwig, L. W. Martin, A. M. Rappe, S.-H. Wei, and J. Perkins, “The 2019 materials by design roadmap,” *Journal of Physics D: Applied Physics*, vol. 52, no. 1, p. 013001, 10 2019.
  - [23] P. V. Balachandran, A. A. Emery, J. E. Gubernatis, T. Lookman, C. Wolverton, and A. Zunger, “Predictions of new perovskite compounds by combining machine learning and density functional theory,” *Physical Review Materials*, vol. 2, p. 43802, 2018.
  - [24] Z. Li, Q. Xu, Q. Sun, Z. Hou, and W.-J. Yin, “Thermodynamic Stability Landscape of Halide Double Perovskites via High-Throughput Computing and Machine Learning,” *Advanced Functional Materials*, vol. 29, no. 9, p. 1807280, 2 2019. [Online]. Available: <http://doi.wiley.com/10.1002/adfm.201807280>
  - [25] J. R. Hattrick-Simpers, K. Choudhary, and C. Corgnale, “A simple constrained machine learning model for predicting high-pressure-hydrogen-compressor materials,” *Cite this: Mol. Syst. Des. Eng.*, vol. 3, p. 509, 2018.
  - [26] D. Jha, L. Ward, A. Paul, W. k. Liao, A. Choudhary, C. Wolverton, and A. Agrawal, “ElemNet: Deep Learning the Chemistry of Materials From Only Elemental Composition,” *Scientific Reports*, vol. 8, no. 1, 12 2018.
  - [27] L. Ward, A. Agrawal, A. Choudhary, and C. Wolverton, “A general-purpose machine learning framework for predicting properties of inorganic materials,” *npj Computational Materials*, vol. 2, 8 2016.
  - [28] D. Jha, K. Choudhary, F. Tavazza, W.-K. Liao, A. Choudhary, C. Campbell, and A. Agrawal, “Enhancing materials property prediction by leveraging computational and experimental data using deep transfer learning.” [Online]. Available: <https://doi.org/10.1038/s41467-019-13297-w>
  - [29] L. Ward, R. Liu, A. Krishna, V. I. Hegde, A. Agrawal, A. Choudhary, and C. Wolverton, “Including crystal structure attributes in machine learning models of formation energies via Voronoi tessellations,” *Physical Review B*, vol. 96, no. 2, 7 2017.

- [30] A. Seko, H. Hayashi, K. Nakayama, A. Takahashi, and I. Tanaka, “Representation of compounds for machine-learning prediction of physical properties,” *Phys. Rev. B*, vol. 95, no. 144110, 2017. [Online]. Available: <https://journals.aps.org/prb/abstract/10.1103/PhysRevB.95.144110>
- [31] K. T. Schütt, H. Glawe, F. Brockherde, A. Sanna, K. R. Müller, and E. K. Gross, “How to represent crystal structures for machine learning: Towards fast prediction of electronic properties,” *Physical Review B - Condensed Matter and Materials Physics*, vol. 89, no. 20, 5 2014.
- [32] C. Rycroft, “Voro++: A three-dimensional voronoi cell library in c++,” Lawrence Berkeley National Lab.(LBNL), Berkeley, CA (United States), Tech. Rep., 2009.
- [33] Y. LeCun, Y. Bengio, and G. Hinton, “Deep learning,” *nature*, vol. 521, no. 7553, pp. 436–444, 2015.
- [34] D. Silver, A. Huang, C. J. Maddison, A. Guez, L. Sifre, G. Van Den Driessche, J. Schrittwieser, I. Antonoglou, V. Panneershelvam, M. Lanctot *et al.*, “Mastering the game of go with deep neural networks and tree search,” *nature*, vol. 529, no. 7587, p. 484, 2016.
- [35] J. Devlin, M.-W. Chang, K. Lee, and K. Toutanova, “Bert: Pre-training of deep bidirectional transformers for language understanding,” *arXiv preprint arXiv:1810.04805*, 2018.
- [36] G. Carleo and M. Troyer, “Solving the quantum many-body problem with artificial neural networks,” *Science*, vol. 355, no. 6325, pp. 602–606, 2017.
- [37] F. Rosenblatt, “The perceptron: a probabilistic model for information storage and organization in the brain.” *Psychological review*, vol. 65, no. 6, p. 386, 1958.
- [38] Y. LeCun, L. Jackel, L. Bottou, A. Brunot, C. Cortes, J. Denker, H. Drucker, I. Guyon, U. Muller, E. Sackinger *et al.*, “Comparison of learning algorithms for handwritten digit recognition,” in *International conference on artificial neural networks*, vol. 60. Perth, Australia, 1995, pp. 53–60.
- [39] Y. LeCun, B. E. Boser, J. S. Denker, D. Henderson, R. E. Howard, W. E. Hubbard, and L. D. Jackel, “Handwritten digit recognition with a back-propagation network,” in *Advances in neural information processing systems*, 1990, pp. 396–404.
- [40] Y. LeCun, L. Bottou, Y. Bengio, and P. Haffner, “Gradient-based learning applied to document recognition,” *Proceedings of the IEEE*, vol. 86, no. 11, pp. 2278–2324, 1998.
- [41] A. Krizhevsky, I. Sutskever, and G. E. Hinton, “Imagenet classification with deep convolutional neural networks,” in *Advances in neural information processing systems*, 2012, pp. 1097–1105.
- [42] V. N. Vapnik, “An overview of statistical learning theory,” *IEEE transactions on neural networks*, vol. 10, no. 5, pp. 988–999, 1999.

- [43] Charles W. Bauschlicher Jr., “A comparison of the accuracy of different functionals,” *Chemical Physics Letters*, vol. 246, pp. 40–44, 11 1995.
- [44] S. Alturk, D. Avci, O. Tamer, and Y. Atalay, “Comparison of different hybrid DFT methods on structural, spectroscopic, electronic and NLO parameters for a potential NLO material,” 2016. [Online]. Available: <http://dx.doi.org/10.1016/j.comptc.2016.12.007>
- [45] T. Hastie, R. Tibshirani, and J. Friedman, *The elements of statistical learning: data mining, inference, and prediction*. Springer Science & Business Media, 2009.
- [46] V. Vapnik, *The nature of statistical learning theory*. Springer science & business media, 2013.
- [47] I. Goodfellow, Y. Bengio, and A. Courville, *Deep learning*. MIT press, 2016.
- [48] X. Glorot and Y. Bengio, “Understanding the difficulty of training deep feedforward neural networks,” in *Proceedings of the thirteenth international conference on artificial intelligence and statistics*, 2010, pp. 249–256.
- [49] V. Nair and G. E. Hinton, “Rectified linear units improve restricted boltzmann machines,” in *ICML*, 2010.
- [50] D.-A. Clevert, T. Unterthiner, and S. Hochreiter, “Fast and accurate deep network learning by exponential linear units (elus),” *arXiv preprint arXiv:1511.07289*, 2015.
- [51] D. P. Kingma and J. Ba, “Adam: A method for stochastic optimization,” *arXiv preprint arXiv:1412.6980*, 2014.
- [52] I. J. Goodfellow, Y. Bulatov, J. Ibarz, S. Arnoud, and V. Shet, “Multi-digit number recognition from street view imagery using deep convolutional neural networks,” *arXiv preprint arXiv:1312.6082*, 2013.
- [53] G. E. Dahl, D. Yu, L. Deng, and A. Acero, “Context-dependent pre-trained deep neural networks for large-vocabulary speech recognition,” *IEEE Transactions on audio, speech, and language processing*, vol. 20, no. 1, pp. 30–42, 2011.
- [54] W. Huang, P. Martin, and H. L. Zhuang, “Machine-learning phase prediction of high-entropy alloys,” *Acta Materialia*, vol. 169, pp. 225–236, 5 2019.
- [55] S. Feng, H. Zhou, and H. Dong, “Using deep neural network with small dataset to predict material defects,” *Materials and Design*, vol. 162, pp. 300–310, 1 2019.
- [56] B. Everitt and A. Skrondal, *The Cambridge dictionary of statistics*. Cambridge University Press Cambridge, 2002, vol. 106.
- [57] A. N. Tikhonov, “On the solution of ill-posed problems and the method of regularization,” in *Doklady Akademii Nauk*, vol. 151, no. 3. Russian Academy of Sciences, 1963, pp. 501–504.



- [58] A. E. Hoerl and R. W. Kennard, “Ridge regression: Biased estimation for nonorthogonal problems,” *Technometrics*, vol. 12, no. 1, pp. 55–67, 1970.
- [59] N. Srivastava, G. Hinton, A. Krizhevsky, I. Sutskever, and R. Salakhutdinov, “Dropout: a simple way to prevent neural networks from overfitting,” *The journal of machine learning research*, vol. 15, no. 1, pp. 1929–1958, 2014.
- [60] C. Tan, F. Sun, T. Kong, W. Zhang, C. Yang, and C. Liu, “A survey on deep transfer learning,” in *International conference on artificial neural networks*. Springer, 2018, pp. 270–279.
- [61] D. C. Cireřan, U. Meier, and J. Schmidhuber, “Transfer learning for latin and chinese characters with deep neural networks,” in *The 2012 International Joint Conference on Neural Networks (IJCNN)*. IEEE, 2012, pp. 1–6.
- [62] H. Chang, J. Han, C. Zhong, A. M. Snijders, and J.-H. Mao, “Unsupervised transfer learning via multi-scale convolutional sparse coding for biomedical applications,” *IEEE transactions on pattern analysis and machine intelligence*, vol. 40, no. 5, pp. 1182–1194, 2017.
- [63] D. George and E. Huerta, “Deep learning for real-time gravitational wave detection and parameter estimation: Results with advanced ligo data,” *Physics Letters B*, vol. 778, pp. 64–70, 2018.
- [64] T. Chen, M. Li, Y. Li, M. Lin, N. Wang, M. Wang, U. W. Cmu, S. Nus, T. Nyu, T. Xiao, B. Xu, C. Zhang, Z. Zhang, and M. U. Alberta, “MXNet: A Flexible and Efficient Machine Learning Library for Heterogeneous Distributed Systems,” Tech. Rep.
- [65] G. Kresse and J. Hafner, “Ab initio molecular dynamics for liquid metals,” *Physical Review B*, vol. 47, no. 1, pp. 558–561, 1993.
- [66] M. Feurer, B. Bocklund, S. Shang, A. Beese, and Z.-K. Liu, “Cr-Fe-Ni Sigma Phase Finite Temperature Calculations,” 2019. [Online]. Available: <https://doi.org/10.25920/yjrc-zj59>
- [67] C.-C. Hsieh and W. Wu, “Overview of Intermetallic Sigma ( $\sigma$ ) Phase Precipitation in Stainless Steels,” vol. 2012, p. 16, 2012.
- [68] A. Zunger, S.-H. Wei, L. G. Ferreira, and J. E. Bernard, “Special Quasirandom Structures,” Tech. Rep. 3, 1990.
- [69] C. Jiang, C. Wolverton, J. Sofo, L.-Q. Chen, and Z.-K. Liu, “First-principles study of binary bcc alloys using special quasirandom structures.”
- [70] D. Shin, R. Arróyave, Z.-K. Liu, and A. Van De Walle, “Thermodynamic properties of binary hcp solution phases from special quasirandom structures.”
- [71] F. Rosenblatt, “The Perceptron—a perceiving and recognizing automaton,” *Report 85-460-1*, 1957.



- [72] N. Srivastava, G. Hinton, A. Krizhevsky, and R. Salakhutdinov, “Dropout: A Simple Way to Prevent Neural Networks from Overfitting,” Tech. Rep., 2014.
- [73] A. Gotmare, N. S. Keskar, C. Xiong, and R. Socher, “A closer look at deep learning heuristics: Learning rate restarts, warmup and distillation,” *arXiv preprint arXiv:1810.13243*, 2018.
- [74] “L2 Regularization.” [Online]. Available: [https://www.textbook.ds100.org/ch/16/reg\\_ridge.html](https://www.textbook.ds100.org/ch/16/reg_ridge.html)
- [75] “POSCAR file.” [Online]. Available: [https://cms.mpi.univie.ac.at/vasp/vasp/POSCAR\\_file.html](https://cms.mpi.univie.ac.at/vasp/vasp/POSCAR_file.html)
- [76] S. R. Hall, F. H. Allen, and I. D. Brown, “The crystallographic information file (CIF): a new standard archive file for crystallography,” *Acta Crystallographica Section A*, vol. 47, no. 6, pp. 655–685, 1991.
- [77] S. P. Ong, W. D. Richards, A. Jain, G. Hautier, M. Kocher, S. Cholia, D. Gunter, V. L. Chevrier, K. A. Persson, and G. Ceder, “Python Materials Genomics (pymatgen): A robust, open-source python library for materials analysis,” *Computational Materials Science*, vol. 68, pp. 314–319, 2 2013. [Online]. Available: <https://linkinghub.elsevier.com/retrieve/pii/S0927025612006295>